Numerical studies of surface and bulk modes in attenuated total reflection spectra*

Yan Bao-Rong(燕保荣)†, Lü Jian-Hong(吕建红),
Kong Ling-Hua(孔令华), and Hu Xi-Wei(胡希伟)

College of Electrical and Electronic Engineering, Huazhong University of Science and Technology, Wuhan 430074, *China*

(Received 3 March 2010; revised manuscript received 7 September 2010)

The dispersion relations of normal modes in the layered constructions are studied. In the frequency region with negative permittivity, we investigate the normal modes near the air–metal and the air–matematerial interfaces and compare them. An extra bulk mode appearing in a pass band of two media is found near the air–matematerial interface, which is different from the air–metal case. Moreover, the bulk mode will be further proved by the attenuated total reflection (ATR) technique, in which the coupling between the incident electromagnetic waves and the normal modes is studied. For p-polarized incident waves, the ATR spectra based on the Otto and the Kretschmann configurations are obtained numerically, where the dips present the excitations of the surface and bulk modes. Furthermore, we also discuss the influences of the middle layer thickness, the incident angle and the damping term on the reflection in detail. It is found that the coupling frequencies and the maximum strength are strongly dependent on the above media parameters.

Keywords: surface polaritons, attenuated total reflection, metamaterial

PACS: 51.70.+f, 78.06.–w, 81.05.–t **DOI:** 10.1088/1674-1056/20/1/015101

1. Introduction

It is well known that air–metal interface can support surface polaritons (SPs).[1,2] This surface mode is a kind of electromagnetic wave bounded at the interface. It is present in the stop band of the metal, in which no mode propagates because of negative permittivity and positive permeability.[3−5] With larger wave-vector, the SPs are explored for their potential applications in subwavelength optics, data storage, light generation, microscopy and bio-photonics.[6] For example, they are used in the miniaturization of nano-optical circuits and the communication devices due to their energy localization.[7] They also play an important role in fabricating the periodically nanostructured metallic films for the enhancement and the directional confinement of light.[8−11] Furthermore, by altering the dimension or the shape of holes on the metal surface, the properties of SPs will be tailored, which offers more potential manipulations.[12,13] Thus, the investigations of SPs are important both from a scientific point of view and from a practical one.[14]

Recently, the SPs retrieve much more attention due to the emergence of metamaterial (MM), which is different from the natural material.[15] A typical MM belongs to left-handed material (LHM) with negative permittivity and negative permeability simultaneously in a certain frequency region, forming a pass band.[16−19] The necessary existence condition of SPs is that signs of the permittivity or the permeability for the two adjacent media are opposite.[3,20] Different from the metal case, the SPs may appear in the pass band of MM.[3] Moreover, an extra mode propagating in the pass bands of both media (called bulk mode in this work) emerges for the MM case. Although this bulk mode is usually ignored by researchers, it influences the attenuated total reflection (ATR) spectra and plays an important role in applications. In the previous work, the ATR method based on the prime coupling[21−23] was used to prove the excitations of surface modes.[24−27] However, the thickness of the middle layer was fixed and the influences of damping, incident angle and other parameters on the spectra were not considered, which was disadvantage for theoretical study and practical applications.

In this work, the ATR spectra of a p-polarized incident wave for air–MM interface are studied and compared with air–metal case, where the emphasis is placed on the influences of the bulk mode on the spectra. Firstly, we investigate the existence regions and the dispersion relations of surface and bulk modes. Secondly, theory of the ATR method is presented,

*Project supported by the National Natural Science Foundation of China (Grant No. 10775055).
†Corresponding author. E-mail: yanbaorong@126.com
© 2011 Chinese Physical Society and IOP Publishing Ltd

where the potential coupling resonant frequencies are obtained. Thirdly, the numerical results of the ATR spectra are presented, where the influences of the middle layer thickness, the incident angle, and the other parameters on the reflection are discussed in detail. Finally, summaries and conclusions are given.

2. Existence regions and dispersion relations of surface and bulk modes

The normal modes are obtained by solving a suitably defined boundary value problem based on the Maxwell's equations. The SPs are essential ones propagating along the interface between two media, whose electric and magnetic fields exponentially decay away from the interface into the bulk of medium on either side. The considered interface is shown in Fig. 1 forming by two infinite media 1 and 2. Medium 1 with electric permittivity ε_1 and magnetic permeability μ_1 occupies the $z > 0$ space, and the region $z < 0$ is occupied by medium 2 with ε_2 and μ_2.

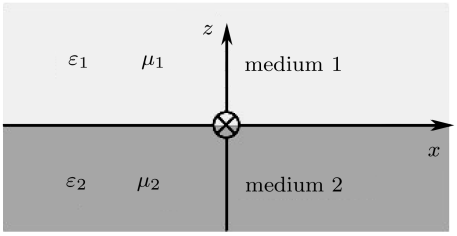


Fig. 1. Configuration of interface between two media and the coordinate system.

Assume that a time harmonic field has frequency ω, then the forms of the magnetic fields along the $\hat{y}$-axis (p-polarized wave) in both media will be given by[28]

$$H(x,y,z) = \begin{cases} \hat{y}H_1 \exp\left[\mathrm{i}k_{x1}x - k_{z1}z - \mathrm{i}\omega t\right], & z > 0, \\ \hat{y}H_2 \exp\left[\mathrm{i}k_{x2}x + k_{z2}z - \mathrm{i}\omega t\right], & z < 0, \end{cases} \tag{1}$$

where $\hat{y}$ is the unit vector and wave-vector components ' $\pm k'_{zi}$ $(i = 1, 2)$ imply an attenuation along the $\hat{z}$-axis. According to the Ampere's law: $\nabla \times H = \varepsilon(\partial E/\partial t)$, the electric fields are obtained as follows:

$$E(x,y,z) = \begin{cases} \left[-\hat{x}\dfrac{H_1 k_{z1}}{\mathrm{i}\omega\varepsilon_1} - \hat{z}\dfrac{H_1 k_{x1}}{\omega\varepsilon_1}\right] \exp\left[\mathrm{i}k_{x1}x - k_{z1}z - \mathrm{i}\omega t\right], & z > 0, \\ \left[\hat{x}\dfrac{H_2 k_{z2}}{\mathrm{i}\omega\varepsilon_2} - \hat{z}\dfrac{H_2 k_{x2}}{\omega\varepsilon_2}\right] \exp\left[\mathrm{i}k_{x2}x + k_{z2}z - \mathrm{i}\omega t\right], & z < 0, \end{cases} \tag{2}$$

where $\hat{x}$ and $\hat{z}$ are the unit vectors. The above wave-vector components are related by equations:

$$k_{x1}^2 - k_{z1}^2 = \varepsilon_1\mu_1\frac{\omega^2}{c^2}, \quad k_{x2}^2 - k_{z2}^2 = \varepsilon_2\mu_2\frac{\omega^2}{c^2}. \tag{3}$$

Then the boundary conditions at the interface require the tangential components of both fields to be continuous, i.e., at $z = 0$,

$$\begin{aligned} &H_1 \exp\left(\mathrm{i}k_{x1}x\right) = H_2 \exp\left(\mathrm{i}k_{x2}x\right), \\ &-\frac{H_1 k_{z1}}{\mathrm{i}\omega\varepsilon_1} \exp\left(\mathrm{i}k_{x1}x\right) = \frac{H_2 k_{z2}}{\mathrm{i}\omega\varepsilon_2} \exp\left(\mathrm{i}k_{x2}x\right). \end{aligned} \tag{4}$$

Therefore the necessary condition for the existence of SPs is

$$\frac{k_{z1}}{\varepsilon_1} + \frac{k_{z2}}{\varepsilon_2} = 0, \tag{5}$$

which implies that two permittivities are opposite. Using Eq. (3), the dispersion relation of normal modes is derived as[28]

$$k_x = \frac{\omega}{c}\left[\frac{\varepsilon_2\varepsilon_1(\varepsilon_2\mu_1 - \varepsilon_1\mu_2)}{\varepsilon_2^2 - \varepsilon_1^2}\right]^{1/2}. \tag{6}$$

Due to the attenuation along the normal direction of interface, the SPs are restricted to regions[3] in which

$$k_x > \max\left[\frac{\omega}{c}\sqrt{\varepsilon_1\mu_1}, \frac{\omega}{c}\sqrt{\varepsilon_2\mu_2}\right], \tag{7}$$

where k_{zi} are real in either medium. Otherwise, the mode with imaginary k_{zi} will propagate in the $\hat{x}\hat{z}$-plane, which is called bulk mode in following.

As an example, the interface constructed by air–metal/MM is investigated to illustrate its normal mode. For metal, the forms of the dispersive permittivity and the permeability are

$$\varepsilon_2 = 1 - \frac{\omega_{\mathrm{p}}^2}{\omega(\omega + \mathrm{i}\gamma_{\mathrm{p}})}, \quad \mu_2 = 1. \tag{8}$$

Here, $\omega_{\rm p}$ is the electric plasma frequency and $\gamma_{\rm p}$ is the damping term of metal. Similarly, the dispersive permittivity and the dispersive permeability of MM will be expressed as[29]

$$\varepsilon_2 = 1 - \frac{\omega_{\rm p}^2}{\omega(\omega + {\rm i}\gamma_{\rm p})} \tag{9}$$

and

$$\mu_2 = 1 - \frac{F\omega^2}{\omega^2 - \omega_0^2 + {\rm i}\omega\Gamma}, \tag{10}$$

respectively when it is composed of periodic arrangements of thin metallic wires and split-ring resonators.[16] The ω_0 in Eq. (10) is the magnetic resonant frequency, constant F is the percentage of the unit cell occupied by the interior of the split ring, and Γ is the damping term. In the following calculations, we only consider the frequency regions with negative permittivity ($\omega < \omega_{\rm p}$). According to Eq. (6), the dispersion curves for the metal and the MM are shown in Figs. 2(a) and 2(b), respectively.

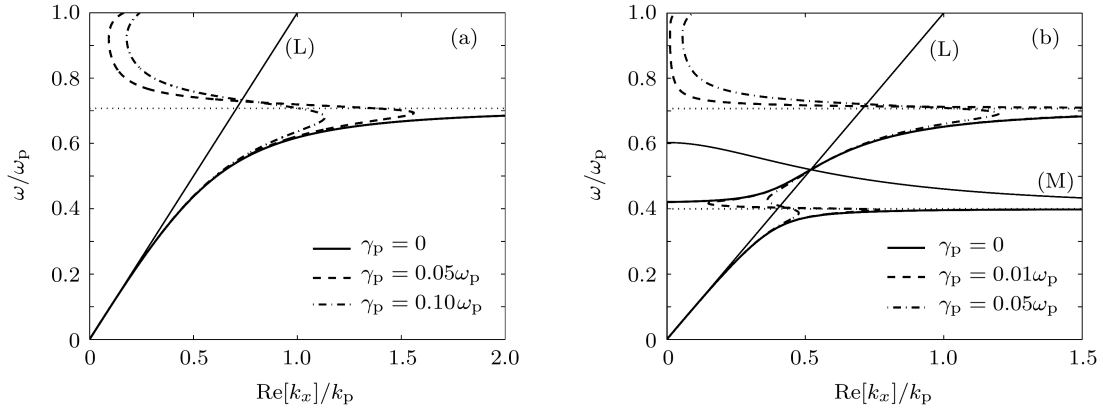


Fig. 2. Calculated dispersion curves for lossless and lossy cases in the plane ($k_x/k_{\rm p}$, $\omega/\omega_{\rm p}$). Panel (a) is for the air–metal interface and panel (b) is for the air–metamaterial interface with $\omega_0 = 0.4\ \omega_{\rm p}$, $F = 0.56$ and $\gamma_{\rm p} = \Gamma$. Line (L) and curve (M) represent the dispersions of light propagating in air and MM, respectively. Here, $k_{\rm p} = \omega_{\rm p}/c$ and the dot horizontal lines represent the resonant frequencies.

First, we discuss the lossless case (without damping). From Fig. 2(a) with $\gamma_{\rm p} = 0$, we can find that there is only one mode lying in the right-hand side of light line (L), which is just a surface mode satisfying Eq. (7). The surface mode resonants at $\omega_{\rm p}/\sqrt{2}$ ($\approx 0.71\ \omega_{\rm p}$) and cannot propagate when $\omega > \omega_{\rm p}/\sqrt{2}$. This surface mode exists in the stop band of metal, owing to negative permittivity and positive permeability. However, there are two branches for the MM case shown in Fig. 2(b). The lower branch on the right-hand side of line (L) is also a surface mode lying in the stop band of MM, where the permittivity and the permeability of MM are opposite. The higher one across the light line (L) is comprised of bulk and surface modes. The part on the right-hand side of line (L) represents a surface mode, which extends from the pass band of MM to the stop band. The other part on the left-hand side represents a bulk mode with imaginary k_{zi}. It can also propagate in MM along the $\hat{z}$-axis because the region where it exists is a pass band of MM with negative permittivity and negative permeability. In addition, Fig. 2(b) shows that there are two resonant frequencies ($0.4\ \omega_{\rm p}$ and $0.71\ \omega_{\rm p}$) and two forbidden regions ($0.4\ \omega_{\rm p} < \omega < 0.42\ \omega_{\rm p}$ and $0.71\ \omega_{\rm p} < \omega < \omega_{\rm p}$).

The influences of medium damping terms $\gamma_{\rm p}$ and Γ on the dispersion are also shown in Fig. 2. Due to the effects of damping, there are anomalous dispersion modes with negative group velocities in the forbidden regions, which evanesce rapidly in the $\hat{x}$ direction with enormous Im$[k_x]$ and finite Re$[k_x]$. Figures 2(a) and 2(b) show that the lossless case and the lossy case of the normal modes present significant differences nearby the resonant frequencies. The effects become distinct with the increase of damping, which will be demonstrated in the ATR spectra in the following sections.

3. Theory of ATR method

The prism-coupling based on the ATR mechanism is an effective technique to detect the excitations of the SPs in multiple layered configuration.[3,4,19] The dips in the ATR spectra imply the coupling (or resonance)

of the incident wave and the normal modes through tunneling effect on the matching condition. The adjunctive wave-vector is supplied by a higher refractive index prism. Usually, the Otto configuration[21] and the Kretschmann configuration[23] are used to investigate the normal modes.

The configuration is a kind of sandwiched structure shown in Fig. 3, where the prism is placed on the top (labeled as 0) and two different media (labeled as 1 and 2) are under the prism in sequence. The permittivity and the permeability of medium i ($i = 0, 1, 2$) are written as ε_i and μ_i, respectively. Generally, the prism and medium 2 are semi-infinite while medium 1 is finite with thickness d. In the Otto geometry (OG), medium 1 is a dielectric with nondispersive permittivity and permeability, while medium 2 is a dispersive one. On the contrary, medium 1 is dispersive and medium 2 is dielectric in the Kretschmann geometry (KG).

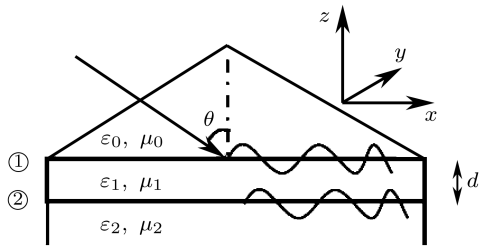


Fig. 3. Configuration of ATR spectra with a prism.

Now, theory of the incident wave coupling to the normal mode based on the above geometry is investigated on the assumption that the dielectric is air and another one is metal or MM. An incident electromagnetic wave comes into the prism with an angle θ, and couples to the normal mode at matching condition, i.e.,

$$\frac{\omega}{c}\sqrt{\varepsilon_0\mu_0}\sin\theta = k_x. \tag{11}$$

The frequencies determined by Eq. (11) are coupling resonant frequencies, which are dependent on incident angle and property of material. For the OG case, surface modes appear only at the interface between media 1 and 2. They are excited by the evanescent wave propagating along the upper interface between the prism and medium 1. The energy is transmitted from the evanescent wave to the surface modes by tunneling effect. In the KG case, surface modes can emerge on the two interfaces of middle layer, but the coupling between the incident wave and the surface mode only occurs near the lower interface. However, there is no significant difference in dispersion curve between the OG and the KG cases.

The dispersion curves and the incident wave at fixed incident angles are shown in Fig. 4, where Fig. 4(a) is for metal and Fig. 4(b) is for MM. Lines (i) and (ii) represent the dispersion of light propagating in the prism for $\theta = 40°$ and $\theta = 50°$, respectively. The solid lines denote the modes near the interface of air–metal/MM, while the dash lines represent the modes near the interface of prism–metal/MM. According to the matching condition Eq. (11), the cross points on the dispersion curves and the incident waves represent the coupling frequencies. The metal used in Fig. 4(a) is silver[30] with $\omega_{\rm p} = 13.7$ PHz. When $\omega < \omega_{\rm p}$, the region under consideration is a stop band of silver. The couplings between the incident wave and the SPs denoted by 'S' occur at 5.5 PHz for 40° and 7.5 PHz for 50°. In Fig. 4(b), the parameters of MM are chosen as $\omega_{\rm p} = 10$ GHz, $\omega_0 = 4$ GHz and $F = 0.56$.[3,25,19]

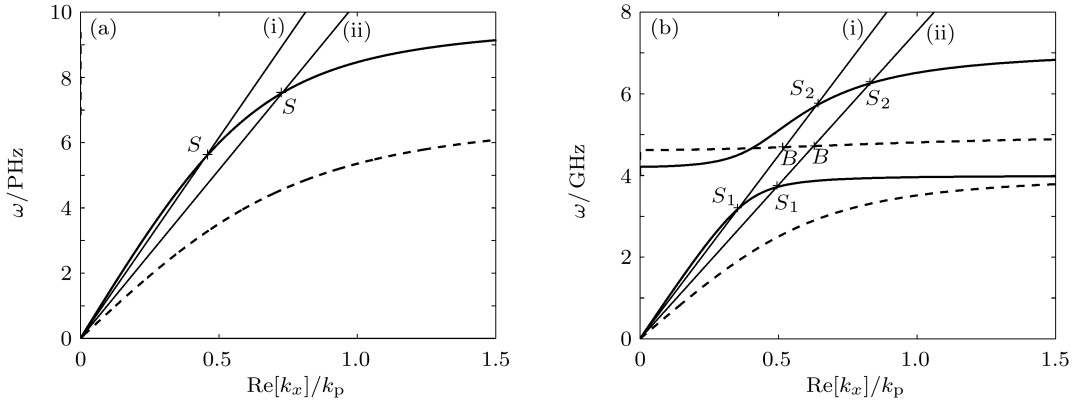


Fig. 4. Dispersion curves in the $(k_x/k_{\rm p}, \omega)$ plane. Lines (i) and (ii) represent the incident waves at 40° and 50°, respectively. The solid curves denote the normal modes of air–medium constructions, while the dash curves refer to those of prism–medium constructions. Panel (a) is for metal and panel (b) is for MM. The intersections denoted 'S' and 'B' show coupling frequencies.

Hence, the MM has the following physical properties. (I) For $\omega < \omega_0$ and $\omega_0/(1-F)^{1/2} < \omega < \omega_p$, i.e., $\omega < 4$ GHz and 6 GHz $< \omega <$10 GHz, it behaves like a metal since the permittivity is negative and the permeability is positive. The regions are the stop bands of MM. (II) Within the range of 4 GHz$< \omega <$6 GHz, it is an LHM since the permittivity and the permeability are both negative, and this frequency range is a pass band of MM. When $\theta = 40°$, two resonant points at 3.2 GHz and 5.7 GHz denoted as 'S_1' and 'S_2' on line (i) represent surface excitations because they both appear in the regions of surface modes. Moreover, there is an extra resonant point at 4.7 GHz denoted by 'B', which represents the coupling between the incident wave and the bulk mode derived from the prism–MM interface. Similarly, the surface couplings at 3.7 GHz and 6.25 GHz and the bulk coupling at 4.72 GHz for 50° are also denoted on line (ii).

4. Numerical calculations of ATR spectra

The ATR spectra for p-polarized wave can be calculated through the classical electromagnetic theory, and the resulting reflectivity form is[25]

$$R = \left| \frac{\gamma_{01} + \gamma_{12} \exp(-2k_{z1}d)}{1 + \gamma_{01}\gamma_{12} \exp(-2k_{z1}d)} \right|^2, \tag{12}$$

where

$$\gamma_{12} = \frac{k_{z2}\varepsilon_1 - k_{z1}\varepsilon_2}{k_{z2}\varepsilon_1 + k_{z1}\varepsilon_2} \tag{13}$$

and

$$\gamma_{01} = \frac{k_{z1}\varepsilon_0 - k_{z0}\varepsilon_1}{k_{z1}\varepsilon_0 + k_{z0}\varepsilon_1}. \tag{14}$$

γ_{12} and γ_{01} are the Fresnel coefficients in the interface when the wave propagates from medium i to medium j. Hereinafter, the influences of thickness d, incident angle θ, damping γ_p and Γ, percentage F on reflectivity R will be studied numerically.

4.1. Metal case

First, the ATR spectra dependent on ω and d at fixed 40° for metal are presented in Fig. 5, where Fig. 5(a) is for the case of OG and Fig. 5(b) is for the case of KG. The damping term $\gamma_p = 90$ THz is used in calculations. Figures 5(a) and 5(b) show that there are obvious coupling zones around 5.5 PHz, which correspond to the 'S' point in Fig. 4(a) approximately. In Fig. 5(a), the minimum reflectivity (i.e., the maximum of coupling strength) appears around $d = 300$ nm. However, it is around $d = 55$ nm in Fig. 5(b). The distance with minimum R is called the optimized coupling distance in the following. Then, Fig. 5 shows that the optimized coupling distance of the KG case is shorter than that of the OG case, which is a result of damping in the middle medium. From Fig. 5, we also find that R increases rapidly with d increasing. In other words, the coupling strength decreases for larger d. The reason is that little energy of the evanescent wave is transferred to the normal modes for larger d, resulting a weaker coupling. On the other hand, if d decreases from the optimized distance, R will increase due to the mismatched complex wave-vector.

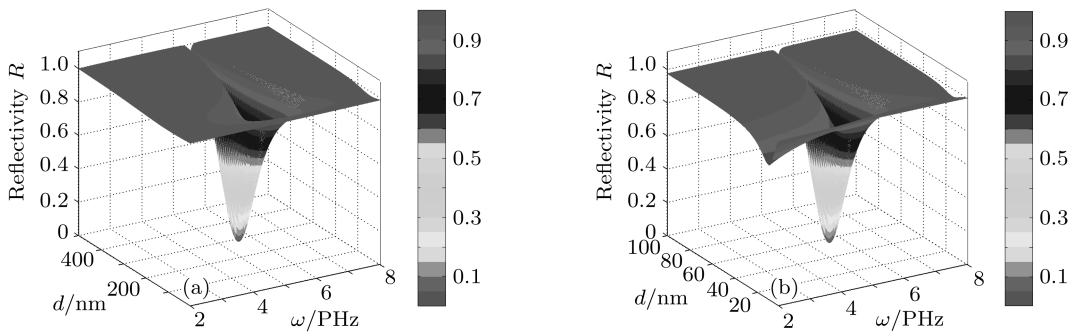


Fig. 5. Calculated R versus frequency ω and thickness d at 40° for (a) Otto configuration and for (b) Krestchmann configuration, where the metal is silver with $\omega_p = 13.7$ PHz and $\gamma_p = 90$ THz.

The spectra of R for the OG case at different combinations of distance d, incident angle θ, and damping γ_p are shown in Figs. 6(a)–6(d). We can find that the coupling frequencies are almost not affected by d and γ_p (see Figs. 6(a), 6(c) and 6(d)), but are markedly changed by the incident angle (see Fig. 6(b)). There is an

optimized distance related to the maximum coupling strength for fixed θ and $\gamma_{\rm p}$. For example, the optimized distance $d = 300$ nm in Fig. 6(a) is in agreement with the result of Fig. 5(a). As also shown in Fig. 6(d), when $\gamma_{\rm p} = 450$ THz, the optimal distance is around $d = 200$ nm. Due to being independent of d, the coupling frequency increases with incident angle shown in Fig. 6(b), which can be interpreted by Fig. 4(a), where the coupling frequency increases with θ since the required matching wave-vector for coupling. When $\theta = 50°$, the coupling occurs around 7.5 PHz, which accords with that on line (ii) in Fig. 4(a). The optimized coupling distance decreases with the increase of incident angle, e.g. $d = 300$ nm for 40° in Fig. 6(a) and $d = 150$ nm for 45° in Fig. 6(b). In the light of Eq. (3), the component k_{z1} monotonically increases with θ, which illustrates faster decay of electromagnetic fields. Then, a smaller optimized distance is reasonable in physics. Figure 6(c) at fixed d shows that R increases and the width well broadens with damping, thereby inducing the damping effect on coupling strength. When we compare Fig. 6(a) with 6(d), the optimized distance decreases for larger damping. The reason may be that the amplitudes of fields decay much faster for a larger damping, which requires a smaller distance to excite the coupling resonance.

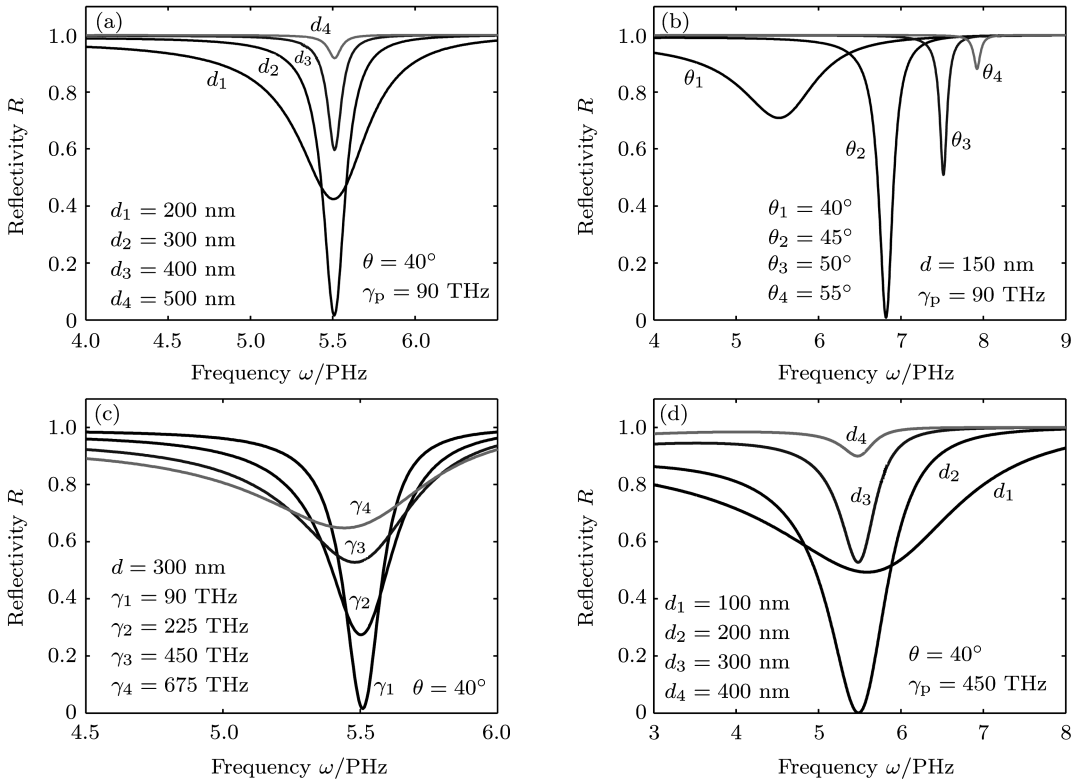


Fig. 6. Calculated R versus ω for the Otto configuration, showing (a) the effect of d at $\theta = 40°$ with $\gamma_{\rm p} = 90$ THz, (b) the effect of θ at $d = 150$ nm and $\gamma_{\rm p} = 90$ THz, (c) the effect of $\gamma_{\rm p}$ with $\theta = 40°$ and $d = 300$ nm, and (d) the effect of d at $\theta = 40°$ with larger damping $\gamma_{\rm p} = 450$ THz.

4.2. Metamaterial case

Now, we replace metal by MM with a lower frequency region. The ATR spectra for MM with dispersive permittivity and permeability in both configurations are described in Fig. 7, where $\gamma_{\rm p} = 0.03\ \omega_{\rm p}$, $\Gamma = 0.03\ \omega_0$ and $\theta = 40°$. There are two dips in ATR spectra near 3.2 GHz and 5.7 GHz, which correspond to the coupling resonant frequencies of the surface modes and the incident wave on line (i) of Fig. 4(b), i.e., 'S_1' and 'S_2'. The corresponding positions of the above two minima for the OG case are around $d = 32$ cm and $d = 15$ cm, respectively, (see Fig. 7(a)). But for the KG case in Fig. 7(b), the minima are around $d = 4.5$ cm and $d = 10$ cm. Similarly, the optimized distances of the KG are smaller than those of the OG due to the damping of MM. Moreover, comparing the component k_{z1} at 3.2 GHz with that at 5.7 GHz, we find that the former is smaller than the latter for the OG, while the situation is exactly opposite to that for the KG. Therefore, the optimized

distance related to 3.2 GHz is larger than that related to 5.7 GHz in Fig. 7(a), and it is opposite to the situation in Fig. 7(b).

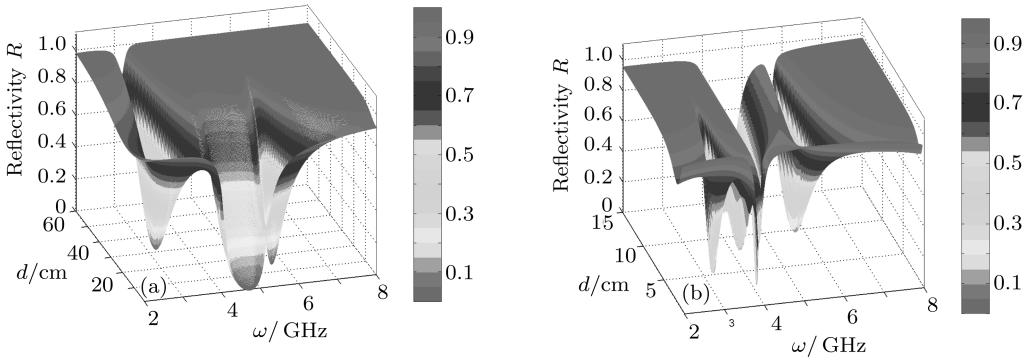
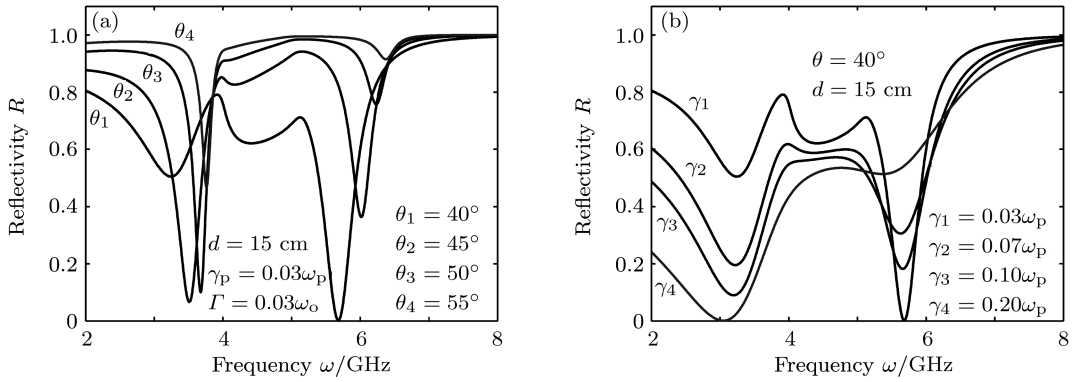


Fig. 7. Calculated R versus ω and middle layer d at 40° for (a) Otto configuration and for (b) Krestchmann configuration. The MM is dispersive with $\omega_{\rm p} = 10$ GHz and the other parameters used in calculations are $\omega_0 = 4$ GHz, $F = 0.56$, $\gamma_{\rm p} = 0.03\ \omega_{\rm p}$ and $\Gamma = 0.03\ \omega_0$.

The most noteworthy characteristic in Fig. 7 is the coupling between the incident wave and the bulk mode, which manifests itself by a dip between two surface mode dips. In the OG case of Fig. 7(a), the coupling between the incident wave and the bulk mode occurs at 4.7 GHz, which is just the 'B' point between 'S_1' and 'S_2' on line (i) of Fig. 4(b). Here, the bulk mode emerging in ATR spectra is derived from the prism–MM interface, so the coupling occurs at smaller d as shown in Fig. 7(a). However, as for the KG case, it is possible for all values of d to excite the bulk coupling, which is proved in Fig. 7(b). When d is smaller, the results are complicated due to the interaction of modes in two surfaces of MM.

For the OG case, the influence of the incident angle θ on the ATR spectra is presented in Fig. 8(a), where d and damping terms are fixed. It is found that the coupling frequencies shift toward higher frequencies with θ increasing, which is determined by the dispersion of SPs and the incident wave, in order to satisfy the wave-vector matching. As shown in Fig. 8(b), the locations of the resonant frequencies seem not to be changed by the damping terms. However, the coupling strength and the optimized distance are dependent on damping, which is similar to the metal case. From Fig. 8(c) for $\gamma_{\rm p} = 0.10\ \omega_{\rm p}$ and $\Gamma = 0.10\ \omega_0$, the optimized distances for the lower (3.2 GHz) and higher (5.7 GHz) coupling frequencies are $d = 20$ cm and $d = 10$ cm respectively, which are smaller than $d = 32$ cm and $d = 15$ cm for $\gamma_{\rm p} = 0.03\ \omega_{\rm p}$ and $\Gamma = 0.03\ \omega_0$ shown in Fig. 7(a). Here, it is reverified that the rate of decay along the normal direction is sensitive to the damping. Figure 8(d) shows that the lower coupling frequency decreases while the higher one increases with F increasing in our calculation. On the other hand, the difference between the two SP resonant frequencies augments with percentage F. If ω_0 is fixed, the dispersion relations change with percentage F since μ_2 is dependent on it. For a larger F, the frequency range of MM with negative ε_2 and μ_2 is increased, which causes a higher coupling frequency. All characteristics of MM in the spectra are useful for designing artificial materials.



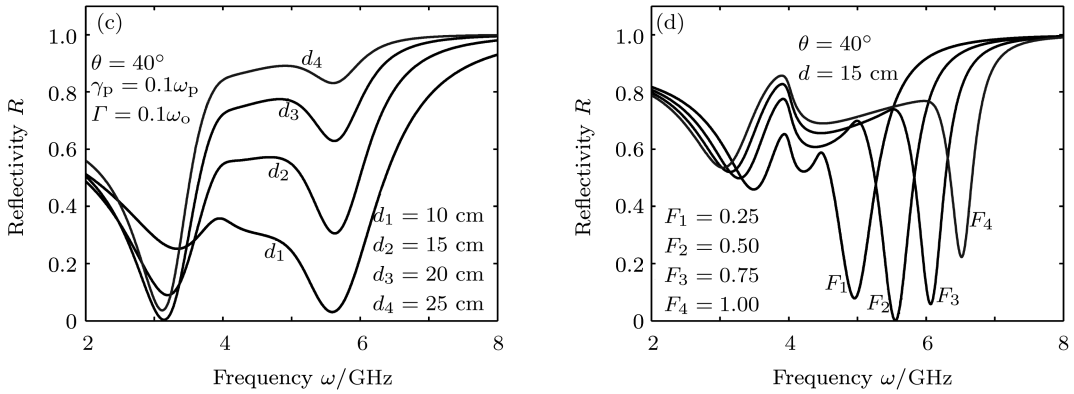


Fig. 8. Calculated R versus ω for MM with $\omega_{\rm p} = 10$ GHz and $\omega_0 = 4$ GHz, showing (a) the effect of θ with $F = 0.56$, (b) the effect of $\gamma_{\rm p}$ and Γ, where the coefficient of Γ is the same as $\gamma_{\rm p}$, (c) the effect of d with larger damping and $F = 0.56$, and (d) the effect of F in MM with $\gamma_{\rm p} = 0.03\ \omega_{\rm p}$ and $\Gamma = 0.03\ \omega_0$.

5. Conclusions

We have theoretically studied the coupling between the incident electromagnetic wave and the normal modes through a multi-layered composite in this paper. Based on the dispersion relations of normal modes near air–metal/MM interface, we find that there is a bulk mode emerging in the pass band of MM, which is different from the metal case. The surface modes and the bulk mode can be recognized from their propagating behaviours.

Then, the ATR spectra are studied numerically. The minima in the spectra correspond to the coupling (resonant excitation) of normal modes, where the SPs and the bulk mode are included for the first time. We have analysed the influences of d, θ, $\gamma_{\rm p}$ (or Γ) and F on the reflectivity and explained the dependence of these parameters briefly. The coupling frequencies are not sensitive to d and $\gamma_{\rm p}$, whereas they are effected by θ and F due to the matching. However, the optimized distances are dependent on $\gamma_{\rm p}$ (or Γ) since they change the rate of field decay along the $\hat{z}$ direction. Comparing the results of the OG and the KG, the discrepancy lies in the bulk coupling, which is valid for smaller d in the former case and for all d's in the latter case. All the discussions should be very useful for understanding and designing artificial materials for various purposes.

References

[1] Raether H 1988 *Surface Plasmons on Smooth and Rough Surfaces and on Gratings* (Berlin: Springer)

[2] Zenneck J 1907 *Ann. Phys.* **23** 846

[3] Ruppin R 2000 *Phys. Lett.* A **277** 61

[4] Ruppin R 2001 *J. Phys.*: *Condens. Matter* **13** 1811

[5] Darmanyan S A, Neviere M and Zakhidov A A 2003 *Opt. Commun.* **225** 233

[6] Barnes W L, Dereux A and Ebbesen T W 2003 *Nature* **424** 824

[7] Marqués R, Martel J, Mesa F and Medina F 2002 *Phys. Rev. Lett.* **89** 183901

[8] Lezec H J, Degiron A, Devaux E, Linke R A, Martin-Moreno L, Garcia-Vidal F J and Ebbesen T W 2002 *Science* **297** 820

[9] Naweed A, Baumann F, Bailey W A, Karakashian A S and Goodhue W D 2003 *J. Opt. Soc. Am.* B **20** 2534

[10] Hua Y L, Fu J X, Li J Y, Li Z Y and Yang H F 2010 *Chin. Phys.* B **19** 047309

[11] Huang Q, Wang J, Cao L R, Sun J, Zhang X D, Geng W D, Xiong S Z and Zhao Y 2009 *Acta Phys. Sin.* **58** 1980 (in Chinese)

[12] Garcia de Abajo F J and Saenz J J 2005 *Phys. Rev. Lett.* **95** 233901

[13] Gay G, Alloschery O, Weiner J, Lezec H J, O'Dwyer C, Sukharev M and Seideman T 2007 *Phys. Rev.* E **75** 016612

[14] Darmanyan S A, Nevière M and Zayats A V 2004 *Phys. Rev.* B **70** 075103

[15] Veselago V G 1968 *Sov. Phys. Usp.* **10** 509

[16] Smith D R, Padilla W J, Vier D C, Nemat-Nasser S C and Schultz S 2000 *Phys. Rev. Lett.* **84** 4184

[17] Lv J H, Yan B R, Liu M H and Hu X W 2009 *Phys. Rev.* E **79** 017601

[18] Lv J H, Yan B R, Liu M H and Hu X W 2009 *Phys. Rev.* E **80** 026605

[19] Zhang H F, Wang Q, Shen N H, Li R, Chen J, Ding J P and Wang H T 2005 *J. Opt. Soc. Am.* B **22** 2686

[20] Park K, Lee B J, Ceji Fu and Zhang Z M 2005 *J. Opt. Soc. Am.* B **22** 1016

[21] Otto A 1968 *Z. Phys.* **216** 398

[22] Otto A 1969 *Z. Phys.* **219** 227

[23] Kretschmann E 1971 *Z. Phys.* **241** 313

[24] Hohenau A, Drezet A, Weissenbacher M, Aussenegg F R and Krenn J R 2008 *Phys. Rev.* B **78** 155405

[25] Tao F, Zhang H F, Yang X H and Cao D 2009 *J. Opt. Soc. Am.* B **26** 50

[26] Chiu K P and Tsai D P 2006 *Proc. SPIE* **6324** 632413

[27] Zhang H F, Cao D, Tao F, Yang X H, Wang Y, Yan X N and Bai L H 2010 *Chin. Phys.* B **19** 027301

[28] Ishimaru A, Jaruwatanadilok S and Kuga Y 2005 *Prog. in Electromagn. Res.* **51** 139

[29] Pendry J B, Holden A J, Stewart W J and Youngs I 1996 *Phys. Rev. Lett.* **76** 4773

[30] Dolling G, Wegener M, Soukoulis C M and Linden S 2007 *Opt. Lett.* **32** 53